Channel coupling effects on the fusion excitation functions for $^{28}Si+^{90,94}Zr$ in sub and near barrier regions

Sunil Kalkal,[1,*] S. Mandal,[1] N. Madhavan,[2] E. Prasad,[3] Shashi Verma,[1] A. Jhingan,[2] Rohit Sandal,[4] S. Nath,[2] J. Gehlot,[2] B. R. Behera,[4] Mansi Saxena,[1] Savi Goyal,[1] Davinder Siwal,[1] Ritika Garg,[1] U. D. Pramanik,[5] Suresh Kumar,[1] T. Varughese,[2] K. S. Golda,[2] S. Muralithar,[2] A. K. Sinha,[6] R. Singh[1,¶]

[1]*Department of Physics and Astrophysics, University of Delhi, Delhi-110007, India*

[2]*Inter University Accelerator Centre, Aruna Asaf Ali Marg, New Delhi-110067, India*

[3]*Department of Physics, Calicut University, Calicut-673635, India*

[4]*Department of Physics, Panjab University, Chandigarh-160014, India.*

[5]*Saha Institute of Nuclear Physics, 1/AF Bidhan Nagar, Kolkata-700064, India*

[6]*UGC-DAE CSR, Kolkata Centre, 3/LB-8, Bidhan Nagar, Kolkata-700098,India*

Fusion excitation functions and angular distributions of evaporation residues (ERs) have been measured for $^{28}Si+^{90,94}Zr$ systems around the Coulomb barrier using the recoil mass spectrometer, Heavy Ion Reaction Analyzer (HIRA). For both the systems, the experimental fusion cross sections are strongly enhanced compared to the predictions of one dimensional barrier penetration model (1-d BPM) below the barrier. Coupled channels formalism has been employed to explain the observed sub-barrier fusion cross section enhancement, theoretically. The enhancement could be explained by considering the coupling of low-lying inelastic states of projectile and target in the $^{28}Si+^{90}Zr$ system. In the sub-barrier region, the measured fusion cross sections for $^{28}Si+^{94}Zr$ turned out to be about an order of magnitude higher than the ones for $^{28}Si+^{90}Zr$ system, which could not be explained by coupling to inelastic states alone. This observation indicates the importance of multi-nucleon transfer reaction channels with positive Q-values in the sub-barrier fusion cross section enhancement as $^{90,94}Zr$ both are believed to have similar collective strengths. This implies that no strong isotopic dependence of fusion cross sections is expected as far as the couplings to collective inelastic states are concerned. In addition, the role of projectile and multi-phonon couplings in the enhancement has been explored.

PACS number(s): 25.70.Jj; 25.70.Hi

¶ Present address: AINST, Amity University, Noida, INDIA.

*kalkal84@gmail.com

I. INTRODUCTION

Understanding the dynamics of heavy ion fusion reactions and interplay of nuclear structure and nuclear reactions has been a subject of intensive study during the last few decades [1-3]. Quite a large enhancement in the sub-barrier heavy ion fusion cross sections (one to two orders of magnitude) over the prediction of 1-d BPM is observed experimentally [1-14]. This enhancement could be explained in terms of coupling of relative motion to internal degrees of freedom of the colliding nuclei associated with specific details of the colliding partners such as deformation [4-6], vibration [7-10] and nucleon transfer channels [11-14] or related to the gross features of nuclear matter such as neck formation [15,16] between the two colliding nuclei. The role of static deformations and collective surface vibrations has been unambiguously established but the precise effect of transfer channels has been seemingly elusive in most of the cases. Inelastic part can be coupled easily but for transfer part, with increasing number of nucleons getting transferred, more and more channels open up, making coupling very much complicated. In order to disentangle the role of transfer channels from collective excitations in enhancement, generally systems, where one target isotope has a closed shell or closed sub-shell and the other one with some nucleons outside the closed shell (so that there are some positive Q-value transfer channels) are selected. In addition, if both of the target nuclei have similar collective strengths, then experimental signature of transfer couplings becomes noticeable while comparing two systems.

The systems which are extensively studied to see the role of transfer channels in the sub-barrier region are ^{40}Ca+^{90,96}Zr [17-19], where a strong interplay of collectivity and transfer in fusion enhancement is observed. But very soon it was realized that ^{96}Zr is a stronger octupole vibrator as compared to ^{90}Zr; the observed enhancement may be due to that rather than transfer channels playing a major role. To verify this, experiments with ^{36}S,^{48}Ca+^{90,96}Zr systems [20, 21] were performed. For all the cases, transfer channels have large negative Q-values. In a more recent experiment, fusion cross sections of ^{40}Ca+^{94}Zr were measured [22] where up to six neutron pick-up channels have positive Q-values. When these cross sections were plotted on a reduced scale, it was found that there was something special about the ^{40}Ca+^{96}Zr system which could be associated with the multi-nucleon transfer channels; the ^{40,48}Ca+^{90}Zr systems have very similar fusion cross sections, and ^{48}Ca+^{96}Zr sub-barrier fusion cross sections were almost a factor of ten higher which could be attributed to the coupling of octupole vibrations of the target nucleus. The ^{40}Ca+^{94,96}Zr fusion cross sections were still higher by up to two orders of magnitude as compared to ^{40,48}Ca+^{90}Zr at the lowest energies [22]. This investigation indicates that the involved fusion reaction dynamics is much more complicated than

simple inclusion of couplings to vibrational states of fusing nuclei and one or two nucleon transfer channels.

In the present paper, we report the measurement of fusion excitation functions for ^{28}Si+^{90,94}Zr systems. The aim of this experiment was to extricate the role of multi-nucleon transfer channels from inelastic excitations as both isotopes have similar quadrupole and octupole strengths, and to investigate the role of the projectile shape and deformation strength in the sub-barrier fusion cross section enhancement. For ^{90}Zr target, fusion excitation function measurements have already been performed using ^{33}S [23], ^{46}Ti [24] (prolate shaped) and ^{36}S [20], ^{50}Ti [24], ^{58}Ni [25] (neutron or proton magic) and ^{40}Ca [19], ^{48}Ca [21] (doubly magic) projectiles. Therefore, an oblate-shaped ^{28}Si nucleus [26] was chosen. Moreover for ^{90,94}Zr, with Z = 40 sub-shell closure, proton transfer channels are not expected to play any significant role. ^{90}Zr is a neutron magic nucleus with the expectation of suppression of neutron pick-up channels owing to the corresponding negative Q-values. The ^{28}Si+^{92}Zr system, on which fusion data already exist in the literature [9], is having only one transfer channel (2n pick-up) with positive Q-value. In case of ^{94}Zr, there are four neutrons outside the closed shell and up to four neutron pick-up channels have positive Q-values. Therefore, it should be possible to clearly observe the effect of single as well as multi-neutron transfer channels in the sub-barrier fusion cross section enhancement by comparing these systems.

II. EXPERIMENTAL DETAILS

The experiment was carried out using pulsed ^{28}Si beam (2 μs repetition rate) from the 15UD Pelletron accelerator at Inter University Accelerator Centre (IUAC), New Delhi. The ^{90,94}Zr targets (having respective enrichments of 97.65% and 96.07%), each with thickness of 280 μg/cm^2 on 45 μg/cm^2 carbon backings were used [27]. Fusion excitation function measurements were carried out using the recoil mass spectrometer, HIRA [28], at laboratory energies (E_{lab}) from 82 to 120 MeV in steps of 2 MeV near the barrier, and 3 to 5 MeV above the barrier covering a range from ~13% below to ~27% above the Coulomb barrier. In the sliding seal target chamber of HIRA, two silicon surface barrier detectors were mounted at angles of $\pm 25^{o}$ with respect to beam direction for normalization to obtain ER cross section and for beam monitoring. A carbon charge reset foil of 35 μg/cm^2 thickness was used 10 cm downstream the target for charge re-equilibration of ERs which may be shifted by internal conversion process. The ERs were dispersed at the focal plane of HIRA according to their m/q values. At the focal plane of HIRA, a position sensitive Multi Wire Proportional Counter (MWPC) with an active area of 150×50 mm^2 was used. For performing the fusion excitation function measurements, HIRA was

kept at 0^o with respect to the beam direction with 5 mSr (+/- 2.28^o) solid angle acceptance. For measuring angular distributions of ERs, HIRA solid angle was changed to 1 mSr and measurements were done in steps of 2^o from 0^o to 10^o, at 103 MeV (E_{lab}) for $^{28}Si+^{90,94}Zr$ systems by rotating HIRA about the beam axis. The timing information in the form of time of flight (TOF) was obtained through a time to amplitude converter with the arrival of particles at the focal plane (MWPC) as the start signal and delayed RF as the stop signal. This TOF was very helpful in separating multiply scattered beam-like particles reaching the focal plane from ERs as shown in Fig. 1. Excellent primary beam rejection and clean separation between beam-like particles and ERs enabled us to measure cross sections down to a few micro barns. At 120 MeV (E_{lab}), HIRA was scanned for charge states, mass and energy of ERs for both the systems [13, 14]. For other incident energies, HIRA fields were scaled appropriately.

In the fusion excitation functions, ER cross section was taken to be the fusion cross section as the fission was negligible for these systems. The ER cross sections were calculated using the expression

$$\sigma_{fus} = \frac{1}{\eta}\left(\frac{Y_{ER}}{Y_M}\right)\left(\frac{d\sigma}{d\Omega}\right)_R \Omega_M$$

where η is average HIRA efficiency for ER detection, Y_{ER} is yield of ERs, Y_M is geometric mean of the monitor yields, $\left(d\sigma/d\Omega\right)_R$ is Rutherford cross section in laboratory and Ω_M is the solid angle subtended by the monitors at the target.

HIRA transmission efficiency was measured by the coincident γ-ray method for $^{28}Si+^{94}Zr$ at 103 MeV (E_{lab}). Singles gamma ray spectrum was taken and then during off-line analysis, TOF gate was put to get γ's which were in coincidence with the particles reaching the focal plane. The ratio of counts for a specific gamma in coincidence spectrum (N_{coin}) to those in singles ($N_{singles}$) spectrum gave transmission efficiency of HIRA for this system. For the identified gamma line (675.2 keV), HIRA efficiency so obtained was 3.2%. Fig. 2 shows coincidence as well as singles gamma spectra. Detection efficiency of ERs depends on the distributions of charge, mass, energy and angle of the particles entering HIRA and on the charge, mass, angular and energy acceptance of HIRA. The distributions are reaction dependent while the physical acceptances are same for all the systems. Absolute detection efficiency for various ERs at all beam energies was calculated by combination of theoretical estimates of charge state distribution (by using Sayer's empirical formula [29]), energy and angular distribution of ERs (by using PACE3 [30]) and mass related efficiency (experimentally measured) as

$$\eta_{HIRA} = \eta_q \eta_E \eta_\theta \eta_m$$

The efficiency so calculated was found to be in very good agreement with that obtained by

gamma-ray method and this method of HIRA efficiency calculation has been adopted in estimating the fusion cross sections. As the ERs were not very far in mass for ^{28}Si+^{90}Zr, similar values were used after checking with simulation program. Theoretical calculations were also performed using a Monte Carlo simulation code TERS [31] and the efficiency obtained by simulation agreed reasonably well with the efficiency obtained experimentally and calculated by PACE3, as given in table I.

III. RESULTS AND DISCUSSION

The measured fusion cross sections for ^{28}Si + ^{90,94}Zr systems are listed in table II. Corrections for loss of beam energy in carbon backing and half target thickness were taken into account. Data for ^{28}Si+^{92}Zr system used in this section are taken from reference [9]. In the present data, the errors are absolute errors consisting of the statistical error and error in HIRA transmission efficiency. For ^{28}Si+^{92}Zr system, only statistical error was taken into account. Coupled channels formalism CCFULL [32], was employed to analyze the data. Various types of potentials had been proposed to explain fusion data over different energy ranges [33-35]. The ion-ion potentials used in these calculations were Woods-Saxon parameterization of Akyuz-Winther (AW) [36] potential. Potential parameters so calculated are listed in table III. These potential parameters have been used without any attempt to vary them to fit the above barrier data. The deformation parameters associated with the transition of multipolarity λ were calculated from measured transition probabilities B (E2) [37] and B (E3) [38] using the expression

$$\beta_{\lambda} = \frac{4\pi}{3ZR^{\lambda}}\sqrt{\left[\frac{B(E\lambda)\uparrow}{e^{2}}\right]}.$$

Here R is radius ($R = r_c A^{1/3}$) of the nucleus which is excited and r_c is taken to be 1.2 fm. The values of β_{λ} so calculated along with the excitation energies of the involved nuclei are given in table IV.

In Fig. 3, measured cross sections for ^{28}Si+^{90}Zr are shown along with the theoretical calculations using CCFULL. The sub-barrier fusion cross sections estimated by 1-d BPM are an order of magnitude smaller than the experimentally measured cross sections. Coupled channels calculations were performed for this system including 2^+, 3^- states of the target one after the other and it was found that 3^- state enhances cross sections more as compared to 2^+ state of target, implying that coupling to 3^- state is stronger in this case. Inclusion of 0^+, 2^+ states of ^{28}Si further increases the sub-barrier fusion cross section. However, if 4^+ state of the projectile is also included in addition, then it over predicts the fusion cross section near as well as below the barrier as shown in Fig. 3(a). A large part of the increase in calculated cross sections is contributed by the strong projectile inelastic excitation. As 3^- state of ^{28}Si is significantly high in energy (6.878 MeV), it is not expected to play any major role [39]. CCFULL

calculations were also performed assuming ^{28}Si as a vibrator, taking 2^+ as a phonon state. But that did not reproduce the data well. It was found that calculations including 2-phonon states of octupole mode (2^+, 3^-, $2^+\otimes 3^-$, $(3^-)^2$, $2^+\otimes(3^-)^2$) in ^{90}Zr and 0^+, 2^+ states of ^{28}Si, reproduced the data reasonably well as shown in Fig. 3(b). Mutual target and projectile excitations were taken into considerations while performing these calculations. In this case, further inclusion of multi-phonon couplings was found to have insignificant effects on the cross sections. The transfer reaction cross sections for the ^{28}Si+^{90}Zr system are expected to be small and, therefore, their influence on the sub-barrier fusion cross section enhancement will be negligible. Though α pick-up channel has small positive Q-value, this channel does not seem to make any significant contribution in the sub-barrier fusion cross section enhancement.

Using the similar coupling scheme as for ^{28}Si+^{90}Zr, coupled channels calculations were performed for ^{28}Si+^{92}Zr system for which fusion cross section data already exist [9]. These calculations along with experimental data points are shown in Fig. 4. It was found that apart from inclusion of inelastic couplings, one has to take into account transfer channel to reproduce the data better. For this system, two neutron pick-up channel has positive Q-value (see table V). The strength of form factor for two particle transfer in CCFULL was varied to explain the experimental data (with equivalent $\beta = 0.30$).

Fusion data of ^{28}Si+^{94}Zr system were analyzed by including several inelastic channels one by one. For this system also, coupling to inelastic excitations predicted cross sections in the sub-barrier region much smaller than experimental values. Even inclusion of 2-neutron pickup was not able to reproduce the experimental cross sections though it enhanced the sub-barrier cross sections to some extent as shown in Fig. 5. In this case, up to four neutron pick up channels have positive Q-values as given in table V. It is clear that one needs to include more transfer channels in this case. As CCFULL provides for an option of including just one pair transfer channel and treats it in too simple a way, therefore, it is not possible to infer the role of transfer channels in the observed enhancement unambiguously. One needs to perform full coupled channels calculations including all the transfer channels appropriately. However, it is observed that the inelastic couplings enhance the sub-barrier fusion cross sections significantly and that too by almost similar amount for each target implying the similarity of low lying states of the ^{90,94}Zr isotopes.

In Fig. 6, a comparative cross section plot for all the systems in the sub- and near-barrier region is shown on a reduced scale. One can see a significant enhancement in the sub-barrier fusion cross sections for ^{28}Si+^{92,94}Zr as compared to ^{28}Si+^{90}Zr system, clearly providing evidence for the role of neutron transfer channels in enhancement. Almost an order of magnitude enhancement is observed in ^{28}Si+^{94}Zr as compared to ^{28}Si+^{92}Zr, giving clear evidence of the role of multi-neutron transfer channels

in fusion cross section enhancement. As it is one neutron transfer might be the most dominant channel as it has the largest cross section. However, from the results reported here, it is clear that even the multi-nucleon transfer channels play a significant role in the enhancement of sub-barrier fusion cross section.

To explore the role of projectile deformation in the enhancement, fusion cross sections of various projectiles with ^{90}Zr target are shown in Fig. 7. When fusion cross sections for all systems divided by square of barrier radius were plotted against energy divided by the barrier height, it was found that the results of 1-d BPM calculations were quite different for each system in the sub-barrier region. Therefore, Wong's expression

$$\sigma_{fus} = \frac{R_b^2 \hbar\omega}{2E_{c.m.}} \ln\left[1+\exp\left(2\pi\frac{E_{c.m.}-V_b}{\hbar\omega}\right)\right],$$

where R_b is barrier radius, $\hbar\omega$ is a measure of barrier curvature, V_b is barrier height, $E_{c.m.}$is energy in centre of mass frame, was used. The σ_{red} and E_{red} were defined as

$$\sigma_{red} = 2\sigma_{fus} E_{c.m.} \Big/ R_b^2 \hbar\omega$$
$$E_{red} = \left(E_{c.m.} - V_b\right)/\hbar\omega.$$

To match the results of 1-d BPM, σ_{red} vs. E_{red} were plotted for all the systems in entire energy range. The values of V_b, $\hbar\omega$ and R_b were obtained by using AW potential parameters in CCFULL calculations. One more thing to be noted is that in all the cases shown in Fig. 7, most of the transfer channels have negative Q-values. Hence, transfer channels will play an insignificant role in enhancing the sub-barrier fusion cross sections for these systems. Out of these projectiles, ^{40,48}Ca are doubly magic, ^{58}Ni is proton magic, ^{50}Ti and ^{36}S are neutron magic whereas ^{28}Si, ^{33}S and ^{46}Ti are mid shell nuclei. Among the mid shell nuclei, ^{28}Si is oblate deformed ($\beta_2 = -0.407$) whereas ^{33}S ($\beta_2 = 0.282$) and ^{46}Ti ($\beta_2 = 0.317$) are prolate deformed nuclei. Deformation parameter for ^{33}S is taken as the average of ^{32}S and ^{34}S. It can be clearly seen from Fig. 7 that the reduced excitation functions involving doubly magic nuclei and magic nuclei (proton or neutron) have same slopes. In the case of ^{58}Ni+^{90}Zr, the experimental data points are lower than the predictions of 1-d BPM. This was found to be so in the original paper too [25]. All the mid shell nuclei have different slopes.

In Fig. 8, ΔE_{red}, the difference in the values of E_{red} corresponding to the experimental cross sections (at 0.1 mb level) for various systems and E_{red} corresponding to 0.1 mb fusion cross section as obtained by 1-d BPM calculations, vs. product of the atomic numbers of colliding nuclei are plotted. It can be seen that all the systems with magic and doubly magic projectiles have a different slope as compared to the systems with mid shell projectiles. For mid shell projectiles, slope is much steeper

than for the magic or doubly magic projectiles implying that the observed enhancement in the sub-barrier fusion cross section increases rapidly with the product of atomic numbers of colliding nuclei for systems with deformed projectiles. For ^{28}Si+^{90}Zr system, the difference is minimum contradictory to expectations if it is a highly deformed oblate nucleus and if projectile plays a major role in the sub-barrier fusion cross section enhancement.

IV. SUMMARY

Fusion excitation functions were measured for ^{28}Si+^{90,94}Zr systems to explore the role of multi-nucleon transfer channels and projectile deformation in the sub-barrier fusion cross section enhancement. Both the targets have similar quadrupole and octupole strengths. The angular distributions of ERs and transmission efficiency of HIRA were also measured at 103MeV (E_{lab}). It was found that for ^{28}Si+^{90,94}Zr systems, AW potential parameters were able to reproduce the data reasonably well at all energies. Reasonable fits to the fusion excitation functions for ^{28}Si+^{90}Zr were obtained by coupling to various inelastic states of the projectile and target. Mutual excitations between target and projectile were also taken into account. It was found that taking ^{28}Si as oblate deformed nucleus could explain the data reasonably well rather than taking it as a vibrator. The role of multi-phonon couplings was also probed for these systems and was found to be of little significance. The ^{28}Si+^{92}Zr data, which were already available in the literature, were analyzed using similar inelastic coupling scheme. It was found that these data were better reproduced by including two neutron pick-up channel. As far as ^{28}Si+^{94}Zr system is concerned, even inclusion of two nucleon transfer channel was not able to explain the data and in fact, still a large enhancement remained unexplained. It seems as if multi-nucleon transfer channels are playing a major role in the observed enhancement for this system. A comparison between ^{28}Si+^{92}Zr and ^{28}Si+^{94}Zr systems gives a clear indication of the importance of multi-neutron pick-up channels in the observed enhancement. Independent of CCFULL calculations, the trend of the data supports the fact that multi-nucleon transfer channels with positive Q-values play an important role in the sub-barrier fusion cross section enhancement. It was also observed that enhancement in the sub-barrier fusion cross sections increases more rapidly with the product of atomic numbers of colliding nuclei for mid shell projectiles as compared to closed shell projectiles.

ACKNOWLEDGMENTS

We are thankful to the Pelletron staff of IUAC for providing a stable beam. We are indebted to target laboratory staff, especially Mr. S. R. Abhilash, for helping in preparation of good quality isotopic

targets. One of the authors (Sunil Kalkal) gratefully acknowledges the award of research fellowship by CSIR, New Delhi.

References:

[1] M. Dasgupta, D. J. Hinde, N. Rowley, A. M. Stefanini, Annu. Rev. Nucl. Part. Sci. **48,** 401(1998).

[2] S. G. Steadman, M. J. Rhoades-Brown, Annu. Rev. Nucl. Part. Sci. **36,** 649 (1986).

[3] M. Beckerman, Rep. Prog. Phys. **51,** 1047 (1988).

[4] J. R. Leigh, M. Dasgupta, D. J. Hinde, J. C. Mein, C. R. Morton, R. C. Lemmon, J. P. Lestone, J. O. Newton, H. Timmers, J. X. Wei, N. Rowley, Phys. Rev. C **52,** 3151 (1995).

[5] J. D. Bierman, P. Chan, J. F. Liang, M. P. Kelly, A. A. Sonzogni, and R. Vandenbosch, Phys. Rev. Lett. **76,** 1587 (1996).

[6] R. G. Stokstad, E. E. Gross, Phys. Rev. C **23,** 281 (1981).

[7] A. M. Stefanini, G. Fortuna, A. Tivelli, W. Meczynski, S. Beghini, C. Signorini, S. Lunardi, M. Morando, Phys. Rev. C. **30,** 2088 (1984).

[8] A. M. Stefanini, D. Ackermann, L. Corradi, J. H. He, G. Montagnoli, S. Beghini, F. Scarlassara, G. F. Segato, Phys. Rev. C **52,** R1727 (1995).

[9] J. O. Newton, C. R. Morton, M. Dasgupta, J. R. Leigh, J. C. Mein, D. J. Hinde, H. Timmers, K. Hagino, Phys. Rev. C **64,** 064608 (2001).

[10] A. M. Stefanini, D. Ackermann, L. Corradi, D. R. Napoli, C. Petrache, P. Spolaore, P. Bednarczyk, H. Q. Zhang, S. Beghini, G. Montagnoli, L. Mueller, F. Scarlassara, G. F. Segato, F. Soramel, N. Rowley, Phys. Rev. Lett. **74,** 864 (1995).

[11] V. I. Zagrebaev, Phys.Rev. C **67,** 061601 (2003).

[12] V. Yu. Denisov, Eur. Phys. J. A **7,** 87 (2000).

[13] Vandana Tripathi , Lagy T. Baby, J. J. Das, P. Sugathan, N. Madhavan, A. K. Sinha, P. V. Madhusudhana Rao, S. K.Hui, R. Singh, K. Hagino, Phys. Rev. C **65,** 014614 (2001).

[14] Lagy T. Baby, Vandana Tripathi, D. O. Kataria, J. J. Das, P. Sugathan, N. Madhavan, A. K. Sinha, M. C. Radhakrishna, N. M. Badiger, N. G. Puttaswamy, A. M. Vinodkumar, N. V. S. V. Prasad, Phys. Rev. C **56,** 1936 (1997).

[15] C. E. Aguiar, V. C. Barbosa, L. F. Canto, R. Donangelo, Nucl. Phys. **A472,** 571 (1987).

[16] C. E. Aguiar, L. F. Canto, R. Donangelo, Phys. Rev. C **31,** 1969 (1985).

[17] Ning Wang, Xizhen Wu, Zhuxia Li, Phys. Rev. C **67,** 024604 (2003).

[18] G. Montagnoli, S. Beghini, F. Scarlassara, A. M. Stefanini, L. Corradi, C. J. Lin, G. Pollarolo, Aage Winther, Eur. Phys. J. A **15,** 351 (2002).

[19] H. Timrners, L. Corradi, A. M. Stefanini, D. Ackermann, J. H. He, S. Beghini, G. Montagnoli, F. Scarlassara, G. F. Segato, N. Rowley, Phys. Lett. B **399,** 35 (1997).

[20] A. M. Stefanini, L. Corradi, A. M. Vinodkumar, Yang Feng, F. Scarlassara, G. Montagnoli, S. Beghini, M. Bisogno, Phys. Rev. C **62,** 014601 (2000).

[21] A. M. Stefanini, F. Scarlassara, S. Beghini, G. Montagnoli, R. Silvestri, M. Trotta, B. R. Behera, L. Corradi, E. Fioretto, A. Gadea, Y. W. Wu, S. Szilner, H. Q. Zhang, Z. H. Liu, M. Ruan, F. Yang, N. Rowley, Phys. Rev. C **73,** 034606 (2006).

[22] A. M. Stefanini, B. R. Behera, S. Beghini, L. Corradi, E. Fioretto, A. Gadea, G. Montagnoli, N. Rowley, F. Scarlassara, S. Szilner, M. Trotta, Phys. Rev. C **76,** 014610 (2007).

[23] L. Corradi, S. J. Skorka, U. Lenz, K. E. G. Lobner, P. R. Pascholati, U. Quade, K. Rudolph, W. Schomburg, M. Steinmayer, H. G. Thies, G. Montagnoli, D. R. Napoli, A. M. Stefanini, A. Tivelli, S. Beghini, F. Scarlassara, C. Signorini, F. Soramel, Z. Phys. A **335,** 55 (1990).

[24] P. H. Stelson, H. J. Kim, M. Beckerman, D. Shapira, R. L. Robinson, Phys. Rev. C **41,** 1584 (1990).

[25] F. Scarlassara, S. Beghini, F. Soramel, C. Signorini, L. Corradi, G. Montagnoli, D. R. Napoli, A. M. Stefanini, Zhi-Chang Li, Z. Phys. A **338,** 171 (1991).

[26] R. H. Spear, Phys. Reports **73,** 369 (1981).

[27] Sunil Kalkal, S. R. Abhilash, D. Kabiraj, S. Mandal, N. Madhavan, R. Singh, Nucl. Instrum. Methods Phys. Res. A **613,** 190 (2010).

[28] A. K. Sinha, N. Madhavan, J. J. Das, P. Sugathan, D. O. Kataria, A. P. Patro, G. K. Mehta, Nucl. Instrum. Methods Phys. Res. A **339,** 543 (1994).

[29] R. O. Sayer, Rev. Phys. Appl. (Paris) **12,** 1543 (1977).

[30] A. Gavron, Phys. Rev. C **21,** 230 (1980).

[31] S. Nath, Comput. Phys. Commun. **179,** 492 (2008).

[32] K. Hagino, N. Rowley, A. T. Kruppa, Comput. Phys. Commun. **123,** 143 (1999).

[33] G. P. A. Nobre, L. C. Chamon, L. R. Gasques, B. V. Carlson, I. J. Thompson, Phys. Rev. C **75,** 044606 (2007).

[34] K. Siwek-Wilczynska, J. Wilczynski, Phys. Rev. C **64,** 024611 (2001).

[35] A. B. Balantekin, S. Kuyucak, J. Phys. G **23,** 1159 (1997).

[36] R. A. Broglia and A. Winther, *Heavy Ion Reaction Lecture Notes, Volume 1: Elastic and Inelastic Reactions* (Benjamin/Cummings, Reading, 1981).

[37] S. Raman, C. W. Nestor, Jr., P. Tikkanen, At. Data Nucl. Data Tables **78,** 1 (2001).

[38] T. Kibedi, R. H. Spear, At. Data Nucl. Data Tables **80,** 35 (2002).

[39] K. Hagino, N. Takigawa, J. R. Bennett, D. M. Brink, Phys. Rev. C **51,** 3190 (1995).

Tables Captions:

TABLE I. HIRA transmission efficiency of ERs for $^{28}Si+^{94}Zr$ system at 103 MeV (E_{lab}).

TABLE II. Fusion cross sections (σ_{fus}) and errors in cross sections ($\delta\sigma$) at centre of mass energies ($E_{c.m.}$) for $^{28}Si+^{90, 94}Zr$ systems.

TABLE III. The parameters of AW potential (Woods-Saxon form) used in coupled channels calculations for all the systems.

TABLE IV. The deformation parameters, excitation energies along with the spin and parities of the states of the nuclei used in the coupled channels calculations.

TABLE V. The g.s. $\rightarrow$ g.s. Q-values (in MeV) for various transfer channels for $^{28}Si+^{90, 92, 94}Zr$ systems. n, p and α denote neutron, proton and α transfer channels, respectively.

Figures captions:

FIG. 1. A two-dimensional spectrum showing the energy loss of particles in MWPC vs. TOF for ^{28}Si + ^{94}Zr system at 103 MeV (E_{lab}). Both x and y-axes are given in channel numbers.

FIG. 2. Gamma ray spectra: Singles spectrum (above) and coincidence (with ERs) spectrum (below).

FIG. 3. ^{28}Si + ^{90}Zr fusion excitation function along with the theoretical calculations using CCFULL. The results of exact coupled channels calculations including various vibartional states of the target and rotational states of ^{28}Si along with the 1-d BPM calculations.

FIG. 4. ^{28}Si + ^{92}Zr fusion excitation function along with the theoretical calculations using CCFULL. The results of exact coupled channels calculations including various inelastic states of target as well as projectile and two neutron pick-up transfer channel along with the 1-d BPM calculations.

FIG. 5. ^{28}Si + ^{94}Zr fusion excitation function along with the theoretical calculations using CCFULL. The results of exact coupled channels calculations including various inelastic states of target as well as projectile and two neutron pick-up transfer channel along with the 1-d BPM calculations.

FIG. 6. Experimental fusion excitation functions for ^{28}Si + $^{90, 92,94}$Zr on a reduced scale (see text).

FIG. 7. Fusion excitation functions for ^{28}Si,^{33,36}S,^{40,48}Ca,^{46,50}Ti,^{58}Ni + ^{90}Zr systems on a reduced scale to match the 1-d BPM values (see the text). E_{red} and σ_{red} are unitless quantities.

FIG. 8. Plot of ΔE_{red} vs. product of atomic numbers of the colliding nuclei. ΔE_{red} is the difference in the values of E_{red} corresponding to the cross sections (at 0.1 mb level) for various systems and E_{red} corresponding to 0.1 mb fusion cross section as obtained by 1-d BPM calculations (see Fig. 7 and the text). Systems in the hatched area are the ones with closed shell projectiles (proton, neutron or both closed shells).

Tables:

TABLE I.

Evaporation Residue	E_γ (in keV)	Experimental (%)	PACE3 (%)	TERS (Simulation) (%)
^{118}I (41%)	675.6	3.2 ± 0.08	3.67	3.01
^{119}I (15%)	674.6		2.90	2.36

TABLE II.

$E_{c.m.}$ (MeV)	σ_{fus} (mb)	$\delta\sigma$ (mb)
	^{28}Si + ^{90}Zr	
65.7	0.049	0.009
67.3	0.435	0.058
68.9	2.317	0.287
70.4	9.770	1.19
72.0	42.60	5.19
73.6	81.18	9.79
75.2	129.2	15.5
76.7	169.1	20.6
79.1	251.5	31.7
82.2	450.3	85.1
84.6	599.0	110.8
88.5	680.1	125.0
92.4	674.3	126.4

^{28}Si + ^{94}Zr		
63.3	0.037	0.006
65.0	0.201	0.029
66.6	2.160	0.310
68.2	10.70	1.48
69.7	26.57	3.68
71.3	52.04	7.28
72.9	100.2	13.9
74.5	138.8	19.3
76.1	165.4	23.1
77.7	216.0	29.6
80.0	285.6	41.1
83.2	467.7	87.9
85.6	565.0	126.4
89.6	599.2	110.0
93.5	542.0	98.2

TABLE III.

System	V_0 (MeV)	r_0 (fm)	a (fm)
^{28}Si + ^{90}Zr	66.01	1.176	0.659
^{28}Si + ^{92}Zr	66.25	1.176	0.660
^{28}Si + ^{94}Zr	66.49	1.176	0.660

TABLE IV.

Nucleus	J^{π}	E_x (MeV)	β
^{90}Zr	2^+	2.19	0.089
	3^-	2.75	0.211
^{92}Zr	2^+	0.93	0.103
	3^-	2.34	0.174
^{94}Zr	2^+	0.92	0.090
	3^-	2.06	0.193
^{28}Si	2^+	1.78	-0.407
	3^-	6.88	0.280

TABLE V.

System	+1n	+2n	+3n	+4n	+1p	-1p	-1n	-α	+α
^{28}Si + ^{90}Zr	-3.50	-2.20	-7.96	-8.37	-5.60	-6.43	-9.98	-7.92	0.28
^{28}Si + ^{92}Zr	-0.16	3.25	-2.13	-2.24	-6.65	-5.54	-10.44	-7.22	3.99
^{28}Si + ^{94}Zr	0.25	4.13	2.08	4.09	-7.58	-4.78	-10.72	-6.71	3.20

Figures:

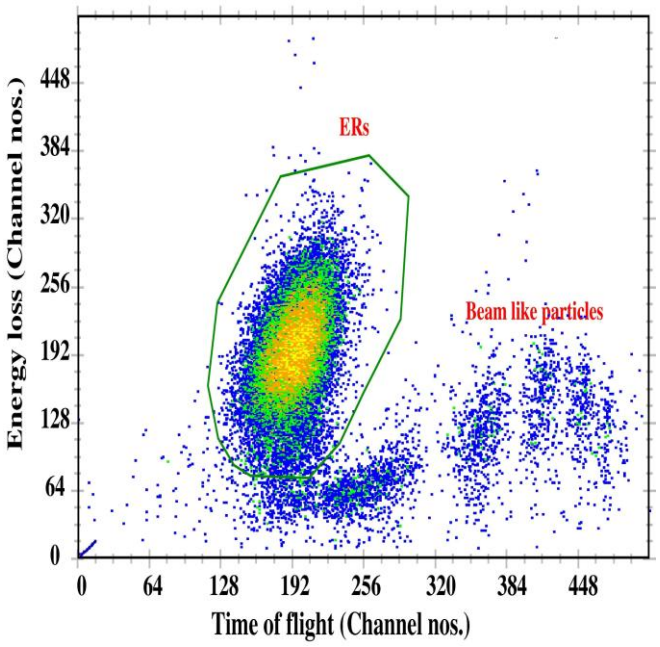

FIG. 1. (Color online).

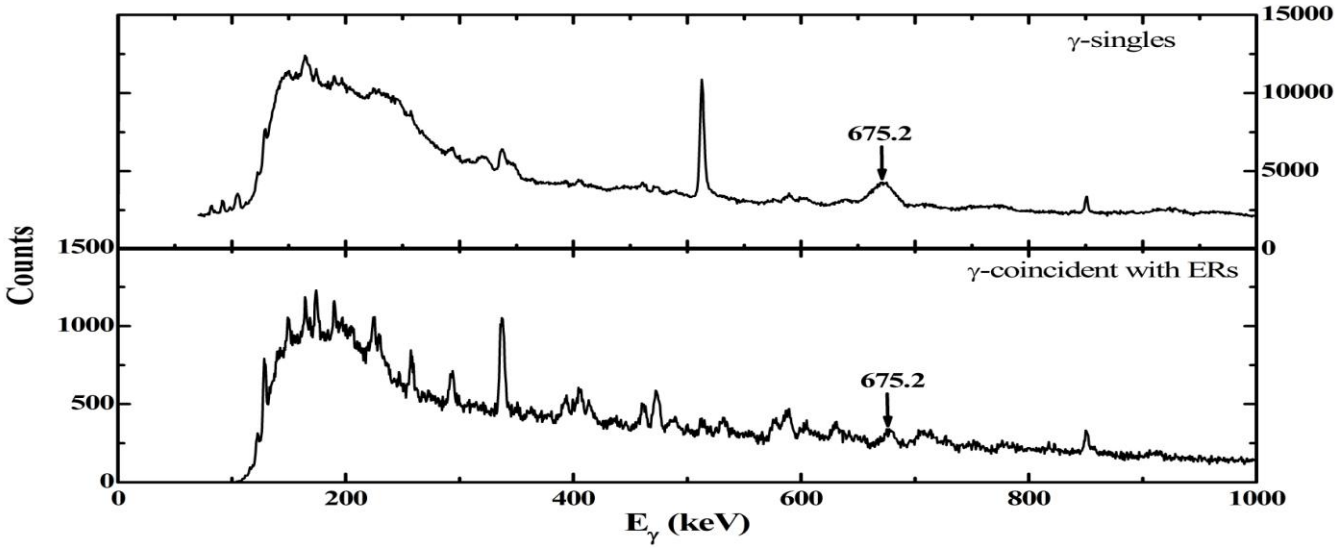
γ-singles
675.2
γ-coincident with ERs
675.2
Counts
E_γ (keV)
15000
10000
5000
0
1500
1000
500
0
0
200
400
600
800
1000

FIG. 2.

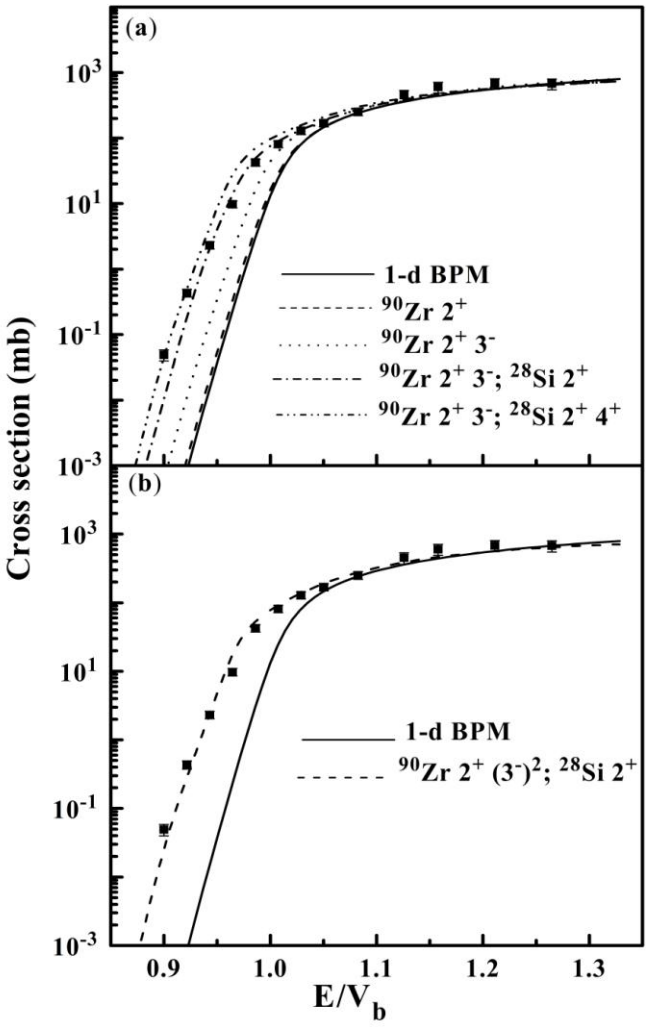
(a)
(b)
Cross section (mb)
E/V_b
1-d BPM
90Zr 2+
90Zr 2+ 3-
90Zr 2+ 3-; 28Si 2+
90Zr 2+ 3-; 28Si 2+ 4+
1-d BPM
90Zr 2+ (3-)2; 28Si 2+

FIG. 3.

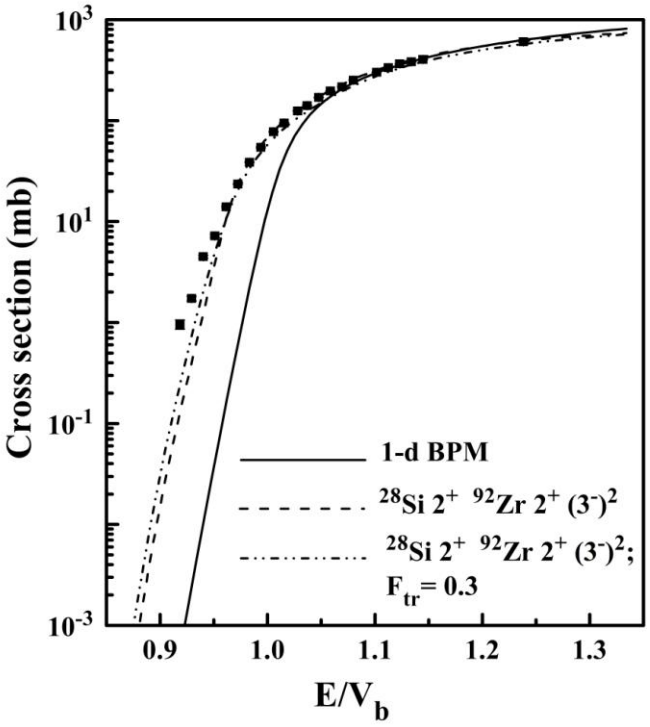
Cross section (mb)
10^3
10^1
10^{-1}
10^{-3}
0.9
1.0
1.1
1.2
1.3
E/V_b
1-d BPM
$^{28}Si\ 2^+\ ^{92}Zr\ 2^+\ (3^-)^2$
$^{28}Si\ 2^+\ ^{92}Zr\ 2^+\ (3^-)^2$;
F_{tr}= 0.3

FIG. 4.

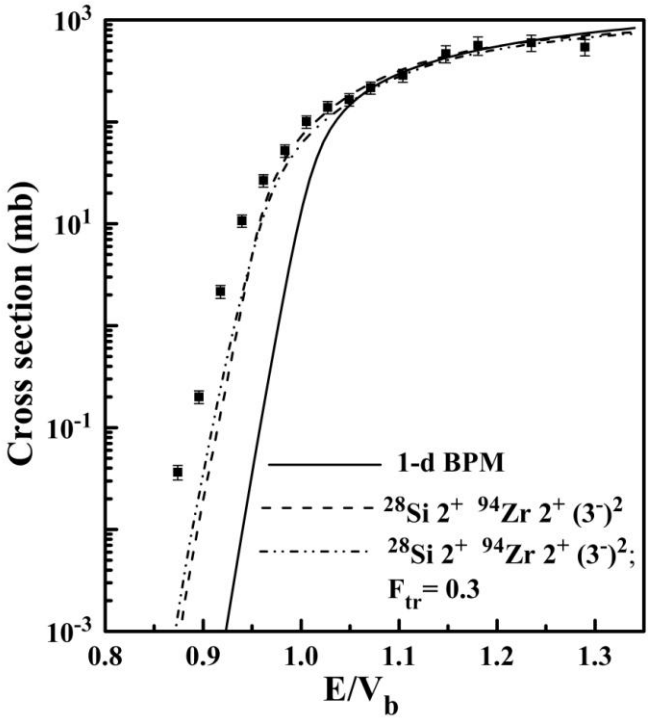
Cross section (mb)
10^3
10^1
10^{-1}
10^{-3}
0.8
0.9
1.0
1.1
1.2
1.3
E/V_b
1-d BPM
$^{28}Si\ 2^+\ ^{94}Zr\ 2^+\ (3^-)^2$
$^{28}Si\ 2^+\ ^{94}Zr\ 2^+\ (3^-)^2$;
F_{tr}= 0.3

FIG. 5.

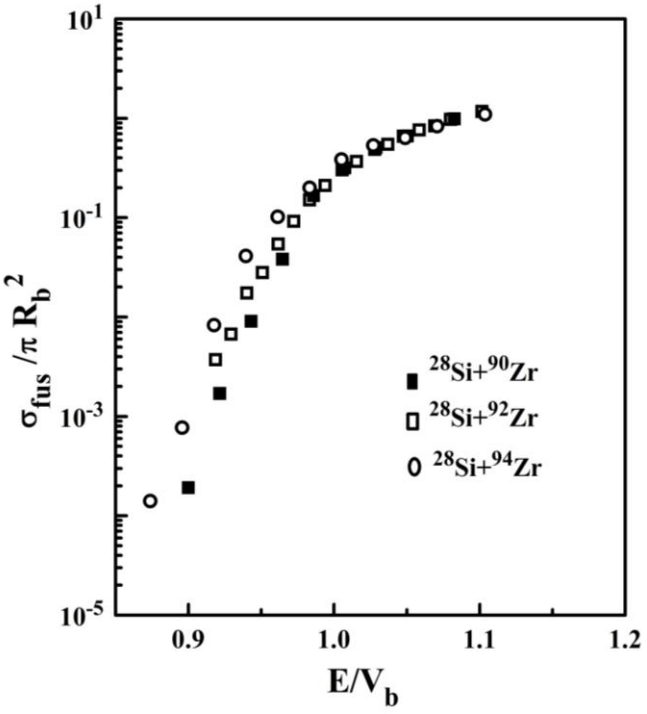
10^1
10^{-1}
10^{-3}
10^{-5}
$\sigma_{fus}/\pi R_b^2$
0.9
1.0
1.1
1.2
E/V_b
$^{28}Si+^{90}Zr$
$^{28}Si+^{92}Zr$
$^{28}Si+^{94}Zr$

FIG. 6.

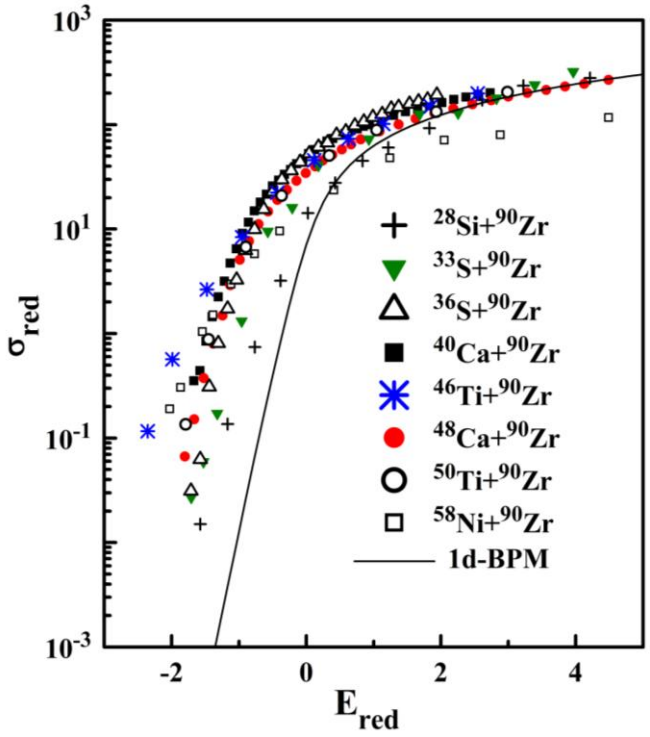

FIG. 7. (Color online).

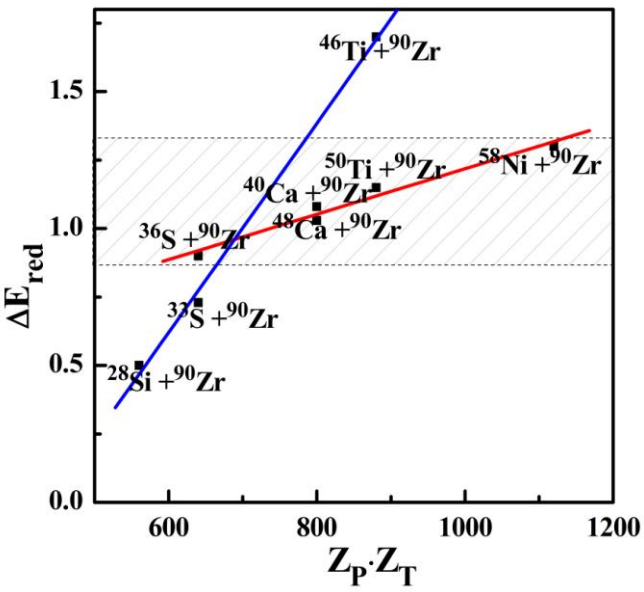

FIG. 8. (Color online).